



HAL
open science

Numerical simulation of a compressible two-layer model: a first attempt with an implicit-explicit splitting scheme

Charles Demay, Christian Bourdarias, Benoît de Laage de Meux, Stéphane Gerbi, Jean-Marc Hérard

► To cite this version:

Charles Demay, Christian Bourdarias, Benoît de Laage de Meux, Stéphane Gerbi, Jean-Marc Hérard. Numerical simulation of a compressible two-layer model: a first attempt with an implicit-explicit splitting scheme. 2016. hal-01421889v1

HAL Id: hal-01421889

<https://hal.science/hal-01421889v1>

Preprint submitted on 23 Dec 2016 (v1), last revised 14 Sep 2018 (v3)

HAL is a multi-disciplinary open access archive for the deposit and dissemination of scientific research documents, whether they are published or not. The documents may come from teaching and research institutions in France or abroad, or from public or private research centers.

L'archive ouverte pluridisciplinaire **HAL**, est destinée au dépôt et à la diffusion de documents scientifiques de niveau recherche, publiés ou non, émanant des établissements d'enseignement et de recherche français ou étrangers, des laboratoires publics ou privés.

Numerical simulation of a compressible two-layer model: a first attempt with an implicit-explicit splitting scheme

Charles Demay^{1,2}, Christian Bourdarias², Benoît de Laage de Meux¹, Stéphane Gerbi², and Jean-Marc Hérard^{1,3}

¹EDF R&D, 6 quai Watier, 78401 Chatou cedex, France

²Laboratoire de Mathématiques, UMR 5127 - CNRS and Université Savoie Mont Blanc, 73376 Le Bourget-du-Lac Cedex, France

³Institut de Mathématiques de Marseille, UMR 7373 - CNRS, Université Aix-Marseille and Centrale Marseille, 13453 Marseille Cedex, France

Abstract

This paper is devoted to the numerical simulation of the compressible two-layer model developed in [16]. The latter is an hyperbolic two-fluid two-pressure model dedicated to gas-liquid flows in pipes, especially stratified air-water flows. Using explicit schemes, one obtains a CFL condition based on the celerity of (fast) acoustic waves which typically brings large numerical diffusivity for the (slow) material waves and small time steps. In order to overcome these drawbacks, the proposed scheme involves an operator splitting and an implicit-explicit time discretization. Thus, the full system is split into two hyperbolic sub-systems. The first one deals with the transport equation on the liquid height using an explicit scheme and upwind fluxes. The second one deals with the averaged mass and momentum conservation equations of both phases using an implicit scheme which handles the propagation of acoustic waves. At last, the positivity of heights and densities is ensured under a CFL condition which involves material velocities. Numerical experiments are performed using acoustic as well as material time steps. Adding the Rusanov scheme for comparison, the best accuracy is obtained with the proposed scheme used with acoustic time steps. When used with *material* time steps, efficiency on the slow waves and stability are obtained regarding analytical solutions of the convective part.

Keywords: Implicit-explicit scheme, operator splitting, two-layer model, gas-liquid flows.

1 Introduction

In this work, we focus on the compressible two-layer model developed in [16]. The latter deals with transient gas-liquid flows in pipes, especially stratified air-water flows which occur in several industrial areas such as nuclear power plants, petroleum industries or sewage pipelines. It is a five-equation system which results from a depth averaging of the isentropic Euler set of equations for each phase where the classical hydrostatic assumption is applied to the liquid. This system is composed by a transport equation on the liquid height in addition to averaged mass and averaged momentum conservation equations for both phases. The derivation process presents similarities with the work exposed in [24]. Thus, the resulting model is a two-fluid two-pressure model and displays the same structure as an isentropic Baer-Nunziato model which provides a statistical description of two-phase flows, especially granular flows or bubbly flows (see for instance [3, 17]). In this context, interesting mathematical properties are obtained such as hyperbolicity, entropy inequality, explicit eigenstructure as well as Riemann invariants and uniqueness of jump conditions. Note that the numerical discretization of this compressible two-layer model has not been considered yet in the literature such that the work presented herein is a first attempt.

From a numerical point of view, the compressible two-layer model, as the isentropic Baer-Nunziato model, are complex to deal with for several reasons. The first difficulty arises from the large size of the system which makes the Riemann problem difficult to solve regarding the convective part and Godunov-type methods. The second difficulty is linked to the presence of non-conservative products in the governing

equations such that the model does not admit a full conservative form. However, the non-conservative products vanish and the system reduces to two decoupled isentropic Euler-type systems on both sides of a linearly degenerate field which is parameterized using the corresponding Riemann invariants. The third difficulty results from the non-linearity in pressure laws which renders even more difficult the derivation of Riemann solvers. When dealing with the full system, one also has to account for relaxation phenomena, in particular pressure relaxation and velocity relaxation given by the source terms, which bring numerical issues regarding the involved time scales.

Despite the mentioned difficulties, some successful solvers are proposed in the literature focusing on the convective part of the Baer-Nunziato system. They are mainly time-explicit Godunov-type methods such as Roe-like scheme, HLL or HLLC scheme and relaxation scheme, see [12, 27, 2, 1, 15, 25] among others. For stability reasons, such methods have to comply with the usual Courant-Friedrichs-Lewy (CFL) condition on the time step which involves the celerity of (fast) acoustic waves and can be very restrictive. In our framework of two-layer pipe flows, even if we are interested in the accurate description of fast waves when the pipe is full of water (in water hammer situation for instance), we are also interested in the dynamics of slow waves associated to material velocities. Thus, an additional difficulty relies in the mix of two types of waves, namely the (fast) acoustic and the (slow) material waves. A possible way to tackle this issue is to use a fractional step method or equivalently an operator splitting. It consists in a multi-step algorithm where each step deals with a system containing exclusively acoustic or material waves. This approach is developed in [4, 6] for the Euler model and in [11] for the isentropic Baer-Nunziato model, among others. Note also that some similarities may be found with the so-called flux splitting approach used in [29] for the Euler model and recently in [28] for the Baer-Nunziato model. However, the above-mentioned references are explicit in time and the CFL condition on the time step still relies on the celerity of fast waves. In order to obtain a less restrictive CFL condition, an implicit-explicit scheme may be used where the fast waves are treated implicitly and the slow waves explicitly to preserve accuracy. Combining the splitting approach and the implicit-explicit treatment, one obtains a CFL condition based on material velocities and consequently a large time-step scheme. This was initially proposed in the context of the Euler model, see [13, 9], and an extension to the Baer-Nunziato model was proposed in [8]. Particularly, the latter references use a Lagrange-Projection approach that consists in approximating the gas dynamics equation using the Lagrange coordinates and then remapping the solution onto an Eulerian mesh. Note that implicit-explicit strategies are also used to derive all speed or all Mach schemes with asymptotic preserving properties regarding the compressible Euler model and its incompressible limit, see [20, 14, 22, 9]. Thus, one can obtain accurate schemes in the low Mach regime with large time steps. Nonetheless, such low Mach properties are still difficult to acquire for two-fluid two-pressure models as the limit model is not clearly defined.

The work presented herein provides numerical results regarding the compressible two-layer model and the related challenges exposed above. Thus, in addition to consider a classical explicit Rusanov scheme known for its robustness, see [30], we propose a large time-step implicit-explicit scheme relying on an operator-splitting approach. The five-equation system is split into two hyperbolic sub-systems. The first one deals with the transport equation on the liquid height using an explicit scheme and upwind fluxes. The second one deals with the averaged mass and momentum conservation equations using an implicit scheme which handles the propagation of acoustic waves. At the end, the positivity of heights and densities is ensured under a CFL condition which involves material velocities. Numerical experiments with grid convergence studies are performed with both schemes using analytical solutions for the convective part of the system. The source terms are then handled accounting for the interactions between the convective dynamics and relaxation phenomena. The dam-break test case is first considered where the numerical solutions are compared with a reference solution given by the incompressible one-layer shallow-water system. Secondly, one considers a so-called mixed flow test case which involves a transition to the pressurized regime (pipe full of water) through a pipe filling.

The paper is organized as follows. The governing equations of the model under consideration are recalled in section 2 as well as its main mathematical properties. Focusing on the convective part of the system, the splitting approach and the associated implicit-explicit scheme are presented in section 3. Numerical experiments are then performed in section 4 building analytical solutions thanks to the available jump conditions and Riemann invariants. In the last part, the full model with the source terms is handled and tested against the dam-break problem and a mixed-flow configuration.

2 The compressible two-layer model

The considered model deals with stratified gas-liquid flows in pipes, see figure 1 for a typical configuration. It results from a depth-averaging of the isentropic Euler set of equations for each phase where the classical hydrostatic assumption is made for the liquid, see [16] for details. The governing equations of the model and its main mathematical properties are exposed below.

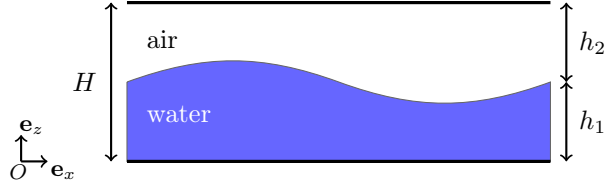


Figure 1: Geometric description for horizontal channels.

2.1 Governing equations

Considering a two-layer air-water flow through an horizontal pipe of height H , see figure 1, the model reads:

$$\frac{\partial h_1}{\partial t} + U_I \frac{\partial h_1}{\partial x} = \lambda_p (P_I - P_2(\rho_2)), \quad (2.1a)$$

$$\frac{\partial h_k \rho_k}{\partial t} + \frac{\partial h_k \rho_k u_k}{\partial x} = 0, \quad (2.1b)$$

$$\frac{\partial h_k \rho_k u_k}{\partial t} + \frac{\partial h_k (\rho_k u_k^2 + P_k(\rho_k))}{\partial x} - P_I \frac{\partial h_k}{\partial x} = (-1)^k \lambda_u (u_1 - u_2), \quad (2.1c)$$

where $k = 1$ for water, $k = 2$ for air, and $h_1 + h_2 = H$. Here, h_k , ρ_k , $P_k(\rho_k)$ and u_k denote respectively the height, the mean density, the mean pressure and the mean velocity of phase k . Surface dynamics is represented by (2.1a) while mass and momentum conservation for each phase are given respectively by (2.1b) and (2.1c).

The interfacial pressure is denoted by P_I and closed by the hydrostatic constraint, while the interfacial velocity is denoted by U_I and closed following an entropy inequality, see section 2.2 and [16] for details. One obtains:

$$(U_I, P_I) = (u_2, P_1 - \rho_1 g \frac{h_1}{2}), \quad (2.2)$$

where g is the gravity field magnitude. As the phases are compressible, state equations are required for gas and liquid pressures. For instance, perfect gas law may be used for air and linear law for water:

$$P_1(\rho_1) = (\rho_1 - \rho_{1,\text{ref}}) c_{1,\text{ref}}^2 + P_{1,\text{ref}}, \quad (2.3a)$$

$$P_2(\rho_2) = P_{2,\text{ref}} \left(\frac{\rho_2}{\rho_{2,\text{ref}}} \right)^{\gamma_2}, \quad (2.3b)$$

with some reference density $\rho_{k,\text{ref}}$ and pressure $P_{k,\text{ref}}$. The celerity of acoustic waves is defined by

$$c_k = \sqrt{P'_k(\rho_k)}, \quad (2.4)$$

where $P'_k(\rho_k) > 0$. For air, γ_2 is set to 7/5 (diatomic gas) and for water, c_1 is constant and equals to a reference celerity denoted $c_{1,\text{ref}}$.

In the following, the thermodynamic reference state is chosen to deal with air-water flows at 20 degrees Celsius: $P_{k,\text{ref}} = 1$ bar, $\rho_{1,\text{ref}} = 998.115$ kg.m⁻³, $c_{1,\text{ref}} = 1500$ m.s⁻¹, $\rho_{2,\text{ref}} = 1.204$ kg.m⁻³ and $c_2 = 350$ m.s⁻¹. Note that phase 1 inherits from the *fastest* pressure waves. Regarding the source terms, λ_p and λ_u are positive bounded functions which account for relaxation time scales, see appendix A for details.

Denoting W the state variable defined as

$$W = (h_1, h_1\rho_1, h_1\rho_1u_1, h_2\rho_2, h_2\rho_2u_2)^T, \quad (2.5)$$

and using (2.2), the system (2.1) may be written under the following condensed form:

$$\frac{\partial W}{\partial t} + \frac{\partial F(W)}{\partial x} + B(W)\frac{\partial W}{\partial x} = C(W), \quad (2.6)$$

where

$$F(W) = \begin{bmatrix} 0 \\ h_1\rho_1u_1 \\ h_2\rho_2u_2 \\ h_1(\rho_1u_1^2 + P_1) \\ h_2(\rho_2u_2^2 + P_2) \end{bmatrix}, \quad B(W)\frac{\partial W}{\partial x} = \begin{bmatrix} u_2\frac{\partial h_1}{\partial x} \\ 0 \\ 0 \\ -(P_1 - \rho_1g\frac{h_1}{2})\frac{\partial h_1}{\partial x} \\ -(P_1 - \rho_1g\frac{h_1}{2})\frac{\partial h_2}{\partial x} \end{bmatrix},$$

and

$$C(W) = \begin{bmatrix} \lambda_p(P_1 - \rho_1g\frac{h_1}{2} - P_2) \\ 0 \\ 0 \\ -\lambda_u(u_1 - u_2) \\ \lambda_u(u_1 - u_2) \end{bmatrix}.$$

As discussed in [16], note that this model is consistent with the shallow water equations as well as the depth-averaged single-phase Euler equations used for pressurized flows. Moreover, its formulation is very close to the isentropic Baer-Nunziato model suited for dispersed flows. Thus, the numerical method exposed in the sequel applies to this other model.

2.2 Mathematical properties

In this section, the main mathematical properties of (2.6) are recalled. Details and proofs are available in [16].

Proposition 2.1 (Entropy inequality). *Smooth solutions of system (2.6) comply with the entropy inequality*

$$\frac{\partial \mathcal{E}}{\partial t} + \frac{\partial \mathcal{G}}{\partial x} \leq 0$$

where the entropy \mathcal{E} and the entropy flux \mathcal{G} are defined by

$$\begin{aligned} \mathcal{E} &= E_{c,1} + E_{p,1} + E_{t,1} + E_{c,2} + E_{t,2}, \\ \mathcal{G} &= u_1(E_{c,1} + E_{p,1} + E_{t,1}) + u_2(E_{c,2} + E_{t,2}) + u_1h_1P_1 + u_2h_2P_2, \end{aligned}$$

with

$$E_{c,k} = \frac{1}{2}h_k\rho_ku_k^2, \quad E_{t,k} = h_k\rho_k\Psi_k(\rho_k), \quad E_{p,1} = \rho_1g\frac{h_1^2}{2},$$

and

$$\Psi'_k(\rho_k) = \frac{P_k(\rho_k)}{\rho_k^2}, \quad k = 1, 2.$$

Proposition 2.2 (Structure of the convective system). *The convective part of (2.6) is hyperbolic under the condition*

$$|u_1 - u_2| \neq c_1.$$

Its eigenvalues are unconditionally real and given by

$$\lambda_1 = u_2, \quad \lambda_2 = u_1 - c_1, \quad \lambda_3 = u_1 + c_1, \quad \lambda_4 = u_2 - c_2, \quad \lambda_5 = u_2 + c_2. \quad (2.7)$$

The field associated with the 1-wave λ_1 is linearly degenerate while the fields associated with the waves λ_k , $k = 2, \dots, 5$, are genuinely nonlinear. Moreover, all the Riemann invariants can be detailed.

Proposition 2.3 (Jump conditions). *Unique jump conditions hold within each isolated field. For all genuine non-linear fields corresponding to the k -waves, $k = 2, \dots, 5$, the Rankine-Hugoniot jump conditions across a single discontinuity of speed σ write*

$$\begin{aligned} [h_k] &= 0, \\ [h_k \rho_k (u_k - \sigma)] &= 0, \\ [h_k \rho_k u_k (u_k - \sigma) + h_k P_k] &= 0, \end{aligned}$$

where brackets $[\cdot]$ denote the difference between the states on both sides of the discontinuity.

Furthermore, as the field associated to the jump of h_1 is linearly degenerate, the non-conservative products $u_2 \partial_x h_1$ and $(P_1 - \rho_1 g \frac{h_1}{2}) \partial_x h_1$ in (2.6) are well defined. Indeed, one may use the available 1-Riemann invariants to write explicitly the 1-wave parametrisation.

Proposition 2.4 (positivity). *Focusing on smooth solutions, the positivity of h_k and ρ_k is verified, as soon as λ_p may be written under the form $\lambda_p = m_1 m_2 \tilde{\lambda}_p$, where $\tilde{\lambda}_p$ is a positive bounded function depending on the state variable. The positivity requirements hold for discontinuous solutions of the Riemann problem associated to the homogeneous system (2.6).*

As the jump conditions and the Riemann invariants can be detailed, recall that one can build analytical solutions for the convective part of (2.6) including the contact discontinuity, shock waves and rarefaction waves. This approach is used in section 4 to verify the numerical scheme exposed in the next section.

3 Splitting method and implicit-explicit scheme for the convective part

In this section, we focus on the convective part of (2.6):

$$\begin{aligned} (\mathcal{S}_0) \quad & \frac{\partial h_1}{\partial t} + u_2 \frac{\partial h_1}{\partial x} = 0, \\ & \frac{\partial m_k}{\partial t} + \frac{m_k u_k}{\partial x} = 0, \\ & \frac{\partial m_k u_k}{\partial t} + \frac{\partial m_k u_k^2}{\partial x} + \frac{\partial h_k P_k}{\partial x} - P_1 \frac{\partial h_k}{\partial x} = 0, \end{aligned}$$

where $m_k = h_k \rho_k$, $k = 1, 2$ and $h_1 + h_2 = H$. More precisely, the goal is to approximate the weak solutions of the associated Cauchy problem with discontinuous initial data:

$$\begin{cases} \frac{\partial W}{\partial t} + \frac{\partial F(W)}{\partial x} + B(W) \frac{\partial W}{\partial x} = 0, & x \in \mathbb{R}, t > 0, \\ W(x, 0) = W_0(x). \end{cases} \quad (3.1)$$

Using classical explicit schemes to discretize (\mathcal{S}_0) and regarding its eigenvalue in (2.7), one obtains a typical CFL condition driven by the fast waves which writes formally:

$$\frac{\Delta t}{\Delta x} \max(|u_2|, |u_1 \pm c_1|, |u_2 \pm c_2|) < 1, \quad (3.2)$$

where Δx and Δt denote respectively the space step and the time step. Dealing with low speed flow, that is $|u_k| \ll |u_k \pm c_k|$, (3.2) may be very constraining and may induce low precision on the material wave (slow wave) which has a leading role in this regime. Thus, the goals of this work is to propose an implicit-explicit scheme more accurate than a classical Rusanov explicit scheme and to examine its ability to relax the CFL condition (3.2). The overall strategy is to split (\mathcal{S}_0) between the material wave λ_1 and the acoustic waves λ_k , $k = 2, \dots, 5$, in order to adapt the numerical treatment: roughly speaking, explicit scheme for the slow wave, implicit scheme for the fast waves. As detailed below, this approach results in CFL conditions which rely on material velocities.

3.1 Splitting approach

It is proposed to split the system (\mathcal{S}_0) into two sub-systems (\mathcal{S}_1) and (\mathcal{S}_2) :

$$\begin{aligned}
 (\mathcal{S}_1) \quad & \frac{\partial h_1}{\partial t} + u_2 \frac{\partial h_1}{\partial x} = 0, \\
 & \frac{\partial m_k}{\partial t} = 0, \\
 & \frac{\partial m_k u_k}{\partial t} = 0. \\
 (\mathcal{S}_2) \quad & \frac{\partial h_1}{\partial t} = 0, \\
 & \frac{\partial m_k}{\partial t} + \frac{\partial m_k u_k}{\partial x} = 0, \\
 & \frac{\partial m_k u_k}{\partial t} + \frac{\partial m_k u_k^2}{\partial x} + \frac{\partial h_k P_k}{\partial x} - P_I \frac{\partial h_k}{\partial x} = 0.
 \end{aligned}$$

A physical interpretation of this splitting can be given in the context of porous flows where h_1 would stand for the porosity. In the first step, one updates the porosity in time and space. In the second step, the porosity is frozen w.r.t. time and the densities and velocities are updated according to this porosity field. In practice, it leads to a splitting of eigenvalues between (\mathcal{S}_1) which contains the material wave and (\mathcal{S}_2) which contains the acoustic waves, with the following properties:

- (\mathcal{S}_1) is *unconditionally hyperbolic*. Its eigenvalues are unconditionally real and given by

$$\begin{aligned}
 \eta_1 &= u_2, \\
 \eta_p &= 0, \quad p = 2, \dots, 5.
 \end{aligned}$$

All the characteristic fields are linearly degenerate.

- (\mathcal{S}_2) is *unconditionally hyperbolic*. Its eigenvalues are unconditionally real and given by

$$\begin{aligned}
 \mu_1 &= 0, \\
 \mu_2 &= u_1 - c_1, \quad \mu_3 = u_1 + c_1, \\
 \mu_4 &= u_2 - c_2, \quad \mu_5 = u_2 + c_2.
 \end{aligned}$$

The field associated with the 1-wave $\mu_1 = 0$ is linearly degenerate while the fields associated with μ_p , $p = 2, \dots, 5$, are genuinely nonlinear.

The numerical strategy is then to use an explicit scheme for (\mathcal{S}_1) and an implicit scheme for (\mathcal{S}_2) .

3.2 Numerical approximation

In the following, we use the operator splitting method in order to derive a fractional-step numerical scheme. The time step Δt and the space step Δx are assumed to be constant for simplicity in the notations. The space is partitioned into cells

$$\mathbb{R} = \bigcup_{i \in \mathbb{N}^*} C_i \text{ with } C_i = [x_{i-\frac{1}{2}}, x_{i+\frac{1}{2}}[, \quad \forall i \in \mathbb{N}^*,$$

where $x_{i+\frac{1}{2}} = (i + \frac{1}{2})\Delta x$ are the cell interfaces. At the discrete times $t^n = n\Delta t$, the solution of (3.1) is approximated on each cell C_i by a constant value denoted by

$$W_i^n = \left((h_1)_i^n, (h_1 \rho_1)_i^n, (h_1 \rho_1 u_1)_i^n, (h_2 \rho_2)_i^n, (h_2 \rho_2 u_2)_i^n \right)^T.$$

The following notation is also introduced:

$$\begin{cases} f^+ = \max(f, 0), \\ f^- = \min(f, 0), \end{cases}$$

such that $f = f^+ + f^-$ and $|f| = f^+ - f^-$.

The first step of the proposed numerical scheme is associated to (\mathcal{S}_1) and updates W_i from W_i^n to W_i^* while the second step is associated to (\mathcal{S}_2) and updates W_i from W_i^* to W_i^{n+1} , each step being associated to the discrete time Δt . The overall numerical scheme is detailed in the next two subsections.

3.3 First step: water height update

In this step, one updates W_i from W_i^n to W_i^* . Regarding the last two equations of (\mathcal{S}_1) , one obtains:

$$m_{k,i}^* = m_{k,i}^n, \quad (3.5)$$

$$(m_k u_k)_i^* = (m_k u_k)_i^n. \quad (3.6)$$

Consequently, $m_{k,i}$ and the velocity $u_{k,i}$ are constant but the density $\rho_{k,i}$ may vary as $h_{k,i}$ may vary.

Writing the transport equation on h_1 under the equivalent form $\frac{\partial h_1}{\partial t} + \frac{\partial u_2 h_1}{\partial x} - h_1 \frac{\partial u_2}{\partial x} = 0$, an explicit first order upwind scheme is proposed:

$$\frac{h_{1,i}^* - h_{1,i}^n}{\Delta t} + \frac{(u_2 h_1)_{i+\frac{1}{2}}^n - (u_2 h_1)_{i-\frac{1}{2}}^n}{\Delta x} - (h_1)_i^n \frac{u_{2,i+\frac{1}{2}}^n - u_{2,i-\frac{1}{2}}^n}{\Delta x} = 0,$$

with

$$\begin{cases} (u_2 h_1)_{i+\frac{1}{2}}^n &= u_{2,i+\frac{1}{2}}^{n,+} h_{1,i}^n + u_{2,i+\frac{1}{2}}^{n,-} h_{1,i+1}^n, \\ u_{2,i+\frac{1}{2}}^n &= \frac{1}{2}(u_{2,i}^n + u_{2,i+1}^n), \end{cases}$$

such that one obtains

$$h_{1,i}^* = \left(1 - \frac{\Delta t}{\Delta x} (u_{2,i-\frac{1}{2}}^{n,+} - u_{2,i+\frac{1}{2}}^{n,-})\right) h_{1,i}^n + \frac{\Delta t}{\Delta x} u_{2,i-\frac{1}{2}}^{n,+} h_{1,i-1}^n - \frac{\Delta t}{\Delta x} u_{2,i+\frac{1}{2}}^{n,-} h_{1,i+1}^n. \quad (3.7)$$

Proposition 3.1 (Positivity of heights). *Regarding (3.7), the positivity of $h_{k,i}^*$ is ensured as soon as the following CFL condition holds*

$$\frac{\Delta t}{\Delta x} \max_i (u_{2,i-\frac{1}{2}}^{n,+} - u_{2,i+\frac{1}{2}}^{n,-}) \leq 1. \quad (3.8)$$

As expected, this CFL condition only depends on material velocities.

3.4 Second step: densities and velocities update

In this step, one updates W_i from W_i^* to W_i^{n+1} . Regarding (\mathcal{S}_2) , the first equation directly yields:

$$h_{1,i}^{n+1} = h_{1,i}^*. \quad (3.9)$$

The proposed time discretization for mass and momentum conservation equations reads:

$$\frac{m_k^{n+1} - m_k^*}{\Delta t} + \frac{\partial(m_k u_k)^{n+1}}{\partial x} = 0, \quad (3.10a)$$

$$\frac{(m_k u_k)^{n+1} - (m_k u_k)^*}{\Delta t} + \frac{\partial(m_k u_k)^{n+1} u_k^*}{\partial x} + h_k^{n+1} \frac{\partial(P_k)^{n+1}}{\partial x} + (P_k - P_l)^{n+1} \frac{\partial(h_k)^{n+1}}{\partial x} = 0. \quad (3.10b)$$

This approach is proposed in order to obtain an implicit equation on ρ_k , or equivalently P_k , and avoid a CFL condition which would involve the celerity of acoustic waves. The current step is divided into two sub-steps where the densities are updated first before updating the velocities using (3.10b).

3.4.1 Densities update

At this stage, it is proposed to neglect the terms $\frac{\partial m_k u_k^2}{\partial x}$ and $(P_k - P_l) \frac{\partial h_k}{\partial x}$ in (3.10b) as they may not be leading terms regarding pressure effects. Thus, (3.10b) becomes:

$$\frac{(m_k u_k)^{n+1} - (m_k u_k)^*}{\Delta t} + h_k^{n+1} \frac{\partial(P_k)^{n+1}}{\partial x} = 0, \quad (3.11)$$

and combining it with (3.10a), one obtains the implicit governing equation of ρ_k which accounts for the propagation of acoustic waves:

$$h_k^{n+1} \rho_k^{n+1} - \Delta t^2 \frac{\partial}{\partial x} \left(h_k^{n+1} \frac{\partial P_k(\rho_k)^{n+1}}{\partial x} \right) = m_k^* - \Delta t \frac{\partial (m_k u_k)^*}{\partial x}. \quad (3.12)$$

After integration on a cell $C_i = [x_{i-\frac{1}{2}}, x_{i+\frac{1}{2}}[$ and using (3.9), it comes:

$$h_{k,i}^* \rho_{k,i}^{n+1} - \frac{\Delta t^2}{\Delta x} \left(\left(h_k^* \frac{\partial (P_k)}{\partial x} \right)^{n+1} \right)_{i+\frac{1}{2}} - \left(h_k^* \frac{\partial (P_k)}{\partial x} \right)^{n+1} \Big|_{i-\frac{1}{2}} = m_{k,i}^* - \frac{\Delta t}{\Delta x} \left((m_k u_k)_{i+\frac{1}{2}}^* - (m_k u_k)_{i-\frac{1}{2}}^* \right),$$

with the corresponding fluxes:

$$\begin{cases} \left(h_k^* \frac{\partial (P_k)}{\partial x} \right)^{n+1} \Big|_{i+\frac{1}{2}} = h_{k,i+\frac{1}{2}}^* \left(\frac{P_{k,i+1}^{n+1} - P_{k,i}^{n+1}}{\Delta x} \right), \\ (m_k u_k)_{i+\frac{1}{2}}^* = u_{k,i+\frac{1}{2}}^{*,+} m_{k,i}^* + u_{k,i+\frac{1}{2}}^{*,-} m_{k,i+1}^*. \end{cases}$$

The implicit system to solve finally writes:

$$\begin{aligned} \left(h_{k,i}^* \frac{\rho_k(P_{k,i}^{n+1})}{P_{k,i}^{n+1}} + \left(\frac{\Delta t}{\Delta x} \right)^2 (h_{k,i+\frac{1}{2}}^* + h_{k,i-\frac{1}{2}}^*) \right) P_{k,i}^{n+1} \\ - \left(\frac{\Delta t}{\Delta x} \right)^2 h_{k,i-\frac{1}{2}}^* P_{k,i-1}^{n+1} - \left(\frac{\Delta t}{\Delta x} \right)^2 h_{k,i+\frac{1}{2}}^* P_{k,i+1}^{n+1} = S_{k,i}^*, \end{aligned} \quad (3.13)$$

where

$$S_{k,i}^* = \frac{\Delta t}{\Delta x} u_{k,i-\frac{1}{2}}^{*,+} m_{k,i-1}^* + \left(1 - \frac{\Delta t}{\Delta x} (u_{k,i+\frac{1}{2}}^{*,+} - u_{k,i-\frac{1}{2}}^{*,-}) \right) m_{k,i}^* - \frac{\Delta t}{\Delta x} u_{k,i+\frac{1}{2}}^{*,-} m_{k,i+1}^*. \quad (3.14)$$

In practice, the interface values $h_{k,i+\frac{1}{2}}^*$ and $u_{k,i+\frac{1}{2}}^*$ are defined by $h_{k,i+\frac{1}{2}}^* = \frac{1}{2}(h_{k,i}^* + h_{k,i+1}^*)$ and $u_{k,i+\frac{1}{2}}^* = \frac{1}{2}(u_{k,i}^* + u_{k,i+1}^*)$. At last, one obtains a non-linear system to solve which is linearized below regarding the choice of the pressure law $P_k(\rho_k)$. As exposed in (2.3), a perfect gas law is used for phase 2 while a linear pressure law is used for phase 1 which applies to air-water flows. In particular, an optimized approach regarding linear pressure laws is used to get the least restrictive CFL condition.

Nonlinear pressure laws

Using the relation $\frac{\partial P_2}{\partial t} = c_2^2(\rho_2) \frac{\partial \rho_2}{\partial t}$, one obtains

$$\rho_{2,i}^{n+1} = \rho_{2,i}^* + \frac{P_{2,i}^{n+1} - P_{2,i}^*}{c_{2,i}^{*2}}. \quad (3.15)$$

Using (3.15), (3.13) is linearized and reads in matrix form:

$$A_2^* \mathbb{P}_2^{n+1} = \mathbb{S}_2^*, \quad (3.16)$$

with

$$A_{2,ij}^* = \begin{cases} \frac{h_{2,i}^*}{c_{2,i}^{*2}} + \left(\frac{\Delta t}{\Delta x} \right)^2 (h_{2,i+\frac{1}{2}}^* + h_{2,i-\frac{1}{2}}^*) & \text{if } i = j, \\ - \left(\frac{\Delta t}{\Delta x} \right)^2 h_{2,i+\frac{1}{2}}^* & \text{if } j = i + 1, \\ - \left(\frac{\Delta t}{\Delta x} \right)^2 h_{2,i-\frac{1}{2}}^* & \text{if } j = i - 1, \\ 0 & \text{elsewhere,} \end{cases}$$

and

$$\begin{aligned} \mathbb{P}_{2,i}^{n+1} &= P_{2,i}^{n+1}, \\ \mathbb{S}_{2,i}^* &= S_{2,i}^* - \left(1 - \frac{1}{\gamma_2} \right) m_{2,i}^*, \end{aligned}$$

where $\gamma_2 = \frac{P_{2,i}^*}{\rho_{2,i}^* c_{2,i}^{*2}} = \frac{7}{5}$ is related to the perfect gas law (2.3b). Note that once (3.16) is solved, one has to use (3.15) to compute $\rho_{2,i}^{n+1}$ instead of the pressure law for consistency reasons.

Linear pressure laws

Using the linearity of the pressure law for phase 1, see (2.3a), (3.13) is already linear. Thus, using $\rho_{1,i}^{n+1}$ instead of $P_{1,i}^{n+1}$ as an unknown, it reads in matrix form:

$$A_1^* \mathbb{R}_1^{n+1} = \mathbb{S}_1^*, \quad (3.17)$$

with

$$A_{1,ij}^* = \begin{cases} h_{1,i}^* + \left(c_1 \frac{\Delta t}{\Delta x}\right)^2 (h_{1,i+\frac{1}{2}}^* + h_{1,i-\frac{1}{2}}^*) & \text{if } i = j, \\ -\left(c_1 \frac{\Delta t}{\Delta x}\right)^2 h_{1,i+\frac{1}{2}}^* & \text{if } j = i + 1, \\ -\left(c_1 \frac{\Delta t}{\Delta x}\right)^2 h_{1,i-\frac{1}{2}}^* & \text{if } j = i - 1, \\ 0 & \text{elsewhere,} \end{cases}$$

and

$$\begin{aligned} \mathbb{R}_{1,i}^{n+1} &= \rho_{1,i}^{n+1}, \\ \mathbb{S}_{1,i}^* &= S_{1,i}^*. \end{aligned}$$

Finally, the densities are updated solving (3.16) and (3.17), the positivity being ensured under the CFL conditions exposed below.

Proposition 3.2 (Positivity of densities). *The positivity of ρ_1^{n+1} is ensured under the following CFL condition:*

$$\frac{\Delta t}{\Delta x} \max_i (u_{1,i+\frac{1}{2}}^{*,+} - u_{1,i-\frac{1}{2}}^{*,+}) \leq 1, \quad (3.18)$$

while the positivity of P_2^{n+1} (and thus ρ_2^{n+1}) is ensured under the following CFL condition:

$$\frac{\Delta t}{\Delta x} \max_i ((u_{2,i+\frac{1}{2}}^{*,+} - u_{2,i-\frac{1}{2}}^{*,+}) \gamma_2) \leq 1, \quad (3.19)$$

where $\gamma_2 = \frac{\rho_{2,i}^* c_{2,i}^{*2}}{P_{2,i}^*} = \frac{7}{5}$ is related to the perfect gas law (2.3b).

Proof. Noting that A_k^* is a M-Matrix:

$$A_{k,ii}^* > 0, \quad A_{k,i \neq j}^* \leq 0, \quad |A_{k,ii}^*| - \sum_j |A_{k,ij}^*| > 0, \quad (3.20)$$

one obtains that A_k^* is nonsingular and $(A_k^{*-1})_{ii} > 0$, which provides:

$$\rho_{k,i}^{n+1} > 0, \forall i \iff \mathbb{S}_k^* > 0. \quad (3.21)$$

Thus, regarding nonlinear pressure laws and \mathbb{S}_2^* , one obtains the CFL condition (3.19). Regarding linear pressure laws, the condition $\mathbb{S}_1^* > 0$ yields (3.18). \square

Finally, dealing with air-water flows, one has to solve (3.16) and (3.17) without violating the CFL conditions (3.19) and (3.18) which involves material velocities.

Remark 3.1. *If (3.19) would apply to phase 1 associated to the linearized pressure law (2.3a), one obtains*

$$\frac{\rho_{1,i}^* c_{1,i}^{*2}}{P_{1,i}^*} = \frac{P_{1,i}^* + \Pi_1}{P_{1,i}^*},$$

where $\Pi_1 = \rho_{1,ref} c_{1,ref}^2 - P_{1,ref}$. When dealing with water and $P_1 \sim 1$ bar, $\frac{P_{1,i}^* + \Pi_1}{P_{1,i}^*} \sim 10^4$ and (3.19) would be very restrictive on $\frac{\Delta t}{\Delta x}$. It is thus profitable to use $\rho_{1,i}^{n+1}$ instead of $P_{1,i}^{n+1}$ as an unknown.

Remark 3.2. Regarding (3.13), one may also propose the approximation $\frac{\rho_k(P_{k,i}^{n+1})}{P_{k,i}^{n+1}} P_{k,i}^{n+1} \approx \frac{\rho_k(P_{k,i}^*)}{P_{k,i}^*} P_{k,i}^{n+1}$ as a linearization process. Thus, one ends up with the following CFL condition:

$$\frac{\Delta t}{\Delta x} \max_i \left(u_{k,i+\frac{1}{2}}^{*,+} - u_{k,i-\frac{1}{2}}^{*,-} \right) \leq 1,$$

which applies to both phases, independently of the pressure law. Note also that (3.13) may be treated as a nonlinear system to solve but it will not be considered here for computational efficiency reasons.

Remark 3.3. One may estimate the condition number $\kappa(A_k)$ of A_k assuming constant heights. Indeed, one obtains a positive-definite matrix whose condition number scales roughly as

$$\kappa(A_k) \sim \frac{1 + 4(c_k \frac{\Delta t}{\Delta x})^2}{1 + \frac{4}{n^2} (c_k \frac{\Delta t}{\Delta x})^2},$$

where n denotes the number of grid points. Under the CFL conditions (3.19) and (3.18), one obtains $\kappa(A_k) \sim n^2$, which is a classical result dealing with the acoustic operator. In the general case, preconditioning techniques may be used to improve the efficiency of the linear solver.

3.4.2 Velocities update

Integrating (3.10a) and (3.10b) on a cell $C_i = [x_{i-\frac{1}{2}}, x_{i+\frac{1}{2}}[$, one obtains:

$$m_{k,i}^{n+1} - m_{k,i}^* + \frac{\Delta t}{\Delta x} \left((m_k u_k)_{i+\frac{1}{2}}^{n+1} - (m_k u_k)_{i-\frac{1}{2}}^{n+1} \right) = 0, \quad (3.22)$$

$$\begin{aligned} (m_k u_k)_i^{n+1} - (m_k u_k)_i^* + \frac{\Delta t}{\Delta x} \left(((m_k u_k)^{n+1} u_k^*)_{i+\frac{1}{2}} - ((m_k u_k)^{n+1} u_k^*)_{i-\frac{1}{2}} \right) \\ + \frac{\Delta t}{\Delta x} \left((h_k P_k)_{i+\frac{1}{2}}^{n+1} - (h_k P_k)_{i-\frac{1}{2}}^{n+1} - P_{I,i}^{n+1} (h_{k,i+\frac{1}{2}}^{n+1} - h_{k,i-\frac{1}{2}}^{n+1}) \right) = 0, \end{aligned} \quad (3.23)$$

where the pressure gradient has been used under its conservative form. At this point, the fluxes $(m_k u_k)_{i+\frac{1}{2}}^{n+1}$ are known using (3.22) but one needs to compute the cell value $(m_k u_k)_i^{n+1}$. To this aim, one considers (3.23) using a first order upwind scheme for $((m_k u_k)^{n+1} u_k^*)_{i+\frac{1}{2}}$ which writes:

$$((m_k u_k)^{n+1} u_k^*)_{i+\frac{1}{2}} = (m_k u_k)_{i+\frac{1}{2}}^{n+1,+} u_{k,i}^* + (m_k u_k)_{i+\frac{1}{2}}^{n+1,-} u_{k,i+1}^*, \quad (3.24)$$

while centered fluxes are used for $(h_k P_k)_{i+\frac{1}{2}}^{n+1}$ and $h_{k,i+\frac{1}{2}}^{n+1}$.

This final step closes the numerical strategy for (\mathcal{S}_0) as all the variables are now updated.

4 Numerical experiments

In this section, we consider two test cases which are Riemann problems built using the available Riemann invariants and the jump conditions. Thus, the analytical solution is known and we compare it with the approximate solution obtained with the proposed implicit-explicit splitting scheme, which is denoted **SP** hereafter. In addition, we add for comparison a classical **Rusanov** explicit scheme applied on (\mathcal{S}_0) .

4.1 Time and space step configurations

4.1.1 Time step profiles

Regarding the **Rusanov** scheme, the associated CFL condition to guarantee the positivity of densities and heights classically writes:

$$\frac{\Delta t_a}{\Delta x} \max_i \left(\frac{r_{i+\frac{1}{2}} + r_{i-\frac{1}{2}}}{2} \right) = \frac{1}{2}, \quad (4.1)$$

where $r_{i+\frac{1}{2}} = \max_{k \in \{1, \dots, 5\}} (|\lambda_{k,i}^n|, |\lambda_{k,i+1}^n|)$, λ_k denoting the eigenvalues of (\mathcal{S}_0) , see (2.7). Note that the CFL number has been chosen to be $\frac{1}{2}$. In our framework, Δt_a will be referred to as the *acoustic* time step as it

contains the celerity of acoustic waves given by $u_k \pm c_k$.

Gathering the CFL conditions (3.8), (3.19), (3.18), the **SP** scheme guarantees the positivity of densities and heights under the condition:

$$\frac{\Delta t_m}{\Delta x} \max_i \left(u_{2,i-\frac{1}{2}}^{n,+} - u_{2,i+\frac{1}{2}}^{n,-}, u_{1,i+\frac{1}{2}}^{*,+} - u_{1,i-\frac{1}{2}}^{*,-}, (u_{2,i+\frac{1}{2}}^{*,+} - u_{2,i-\frac{1}{2}}^{*,-}) \gamma_2 \right) = \frac{1}{2}, \quad (4.2)$$

where the CFL number has been chosen to be $\frac{1}{2}$. In our framework, Δt_m will be referred to as the *material* time step as it contains only material speeds, which consequently yields $\Delta t_a < \Delta t_m$.

In order to evaluate the influence of the time step on the approximated solutions, one introduces two variants for the **SP** scheme:

- **SP_a**: **SP** scheme with the *acoustic* time step Δt_a defined in (4.1).
- **SP_m**: **SP** scheme with the *material* time step Δt_m defined in (4.2).

The two variants are compared with the **Rusanov** scheme whose time step is necessarily the *acoustic* one. To summarize, the time step profiles are sketched on figure 2. Note that a ramp on the CFL number is used in the first iterations to start the calculations.

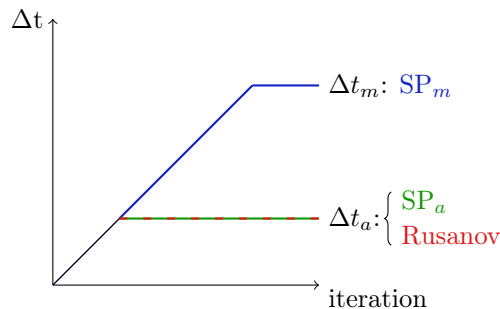


Figure 2: Time step profiles.

4.1.2 Mesh refinement

The solutions are computed on the domain $[0, 1]$ of the x -space where homogeneous Neumann conditions are imposed at the inlet and outlet. A mesh refinement is performed in order to check the numerical convergence of the method. For this purpose, the discrete L^1 -error between the approximate solution and the exact one at the final time T , normalized by the discrete L^1 -norm of the exact solution, is computed:

$$\text{error}(\Delta x, T) = \frac{\sum_j |\mathcal{U}_j^n - \mathcal{U}_{ex}(x_j, T)|}{\sum_j |\mathcal{U}_{ex}(x_j, T)|}, \quad (4.3)$$

where \mathcal{U} denotes the state vector in non conservative variables:

$$\mathcal{U} = (\alpha_1, \rho_1, u_1, \rho_2, u_2),$$

and \mathcal{U}_{ex} stands for the exact solution. Note that Δt is defined from Δx through (4.1) or (4.2). In the refinement process, the coarser mesh is composed of 100 cells and the most refined one contains 200000 cells. Hereafter, the fields are plotted with 1000 cells and the error is plotted against Δx using a *log-log* scale.

4.2 Numerical results

4.2.1 Test case 1: one shock within each phase

In this first test case, one considers one shock within each phase. One shock on phase 2 is traveling at $\lambda_4 = u_2 - c_2$ and linking the left state \mathcal{U}_L to the state \mathcal{U}_C . One shock on phase 1 is traveling at $\lambda_3 = u_1 + c_1$

and linking the state \mathcal{U}_C to the right state \mathcal{U}_R . In particular, there is no contact discontinuity since the initial condition for h_1 is uniform. Thus, it consists in solving two decoupled isentropic Euler systems, see the wave structure and initial conditions on figure 3.

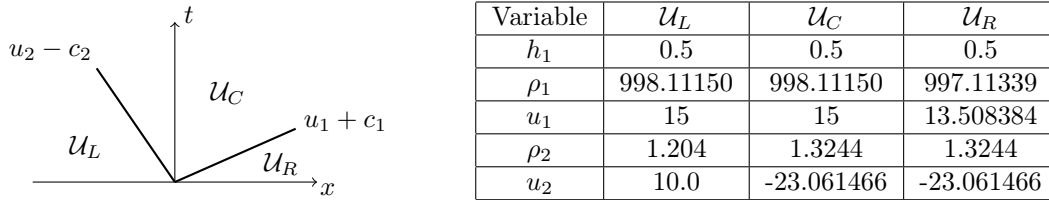


Figure 3: Wave structure, initial conditions (\mathcal{U}_L , \mathcal{U}_R) and intermediate state (\mathcal{U}_C) for test case 1.

The fields at $T = 16.10^{-5}$ s. with 1000 cells and the errors are displayed respectively on figures 4 and 5.

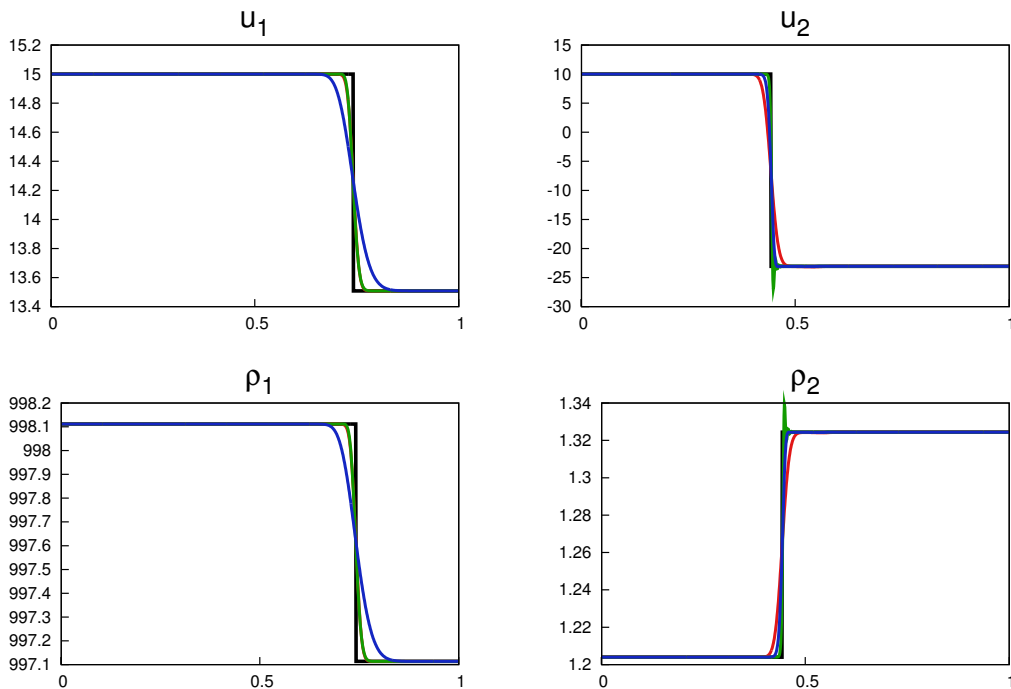


Figure 4: Approximate solution for test case 1 at $T = 16.10^{-5}$ s. with 1000 cells. - Exact solution, - SP_m , - SP_a , - $Rusanov$.

As a first comment, one can see on figure 4 that the different methods approximate the relevant shock solutions. Regarding the fields and the errors for phase 1, the results for SP_a and $Rusanov$ are similar. As phase 1 is the fastest one, $Rusanov$ is in its optimal regime regarding the shock waves and compares well with SP_a . One observes a loss of accuracy with SP_m which is more diffusive around the shock location. Regarding the fields and the errors for phase 2, the best accuracy is obtained with SP_a which is partly due to the centered pressure gradient in the implicit equation (3.13). However, overshoots are observed on the fields but the latter are bounded in L^∞ -norm and do not preclude the convergence. Regarding coarser meshes, SP_m is more accurate than $Rusanov$ and both are comparable when the mesh is refined.

Dealing with isolated shock waves, one would expect to reach a first order convergence rate. This order is obtained for phase 2 but not for phase 1 which displays order $\frac{1}{2}$, see figure 5. As an explanation, note that the shock on density is far weaker for phase 1 (water) than for phase 2 (air). Such configurations are realistic and make the shock more difficult to capture for phase 1.

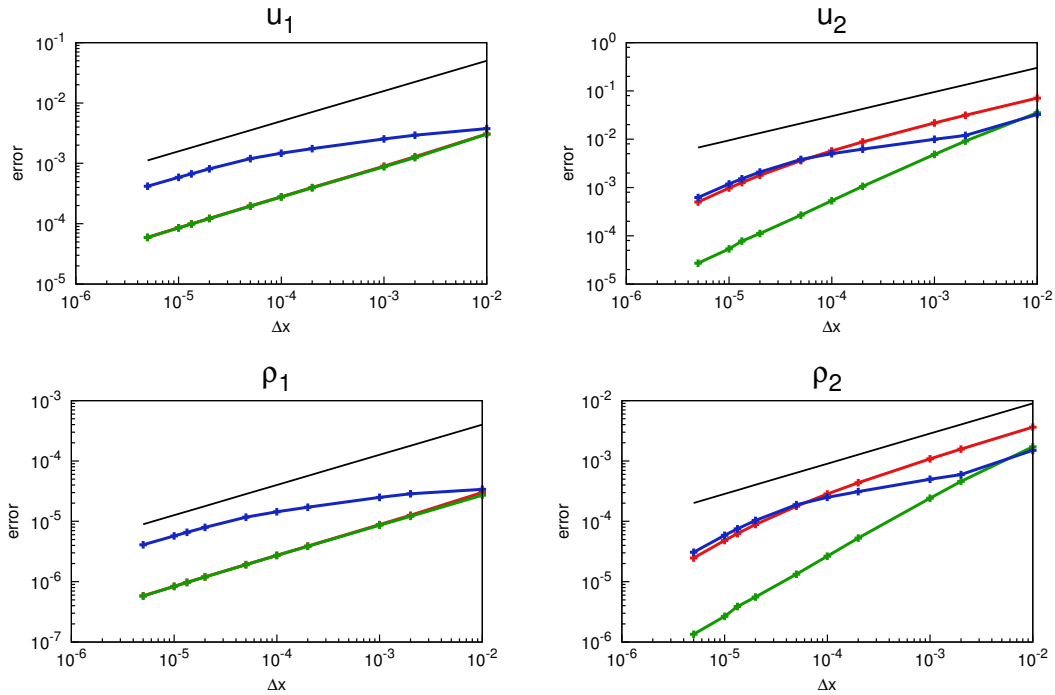


Figure 5: Errors in L^1 -norm for test case 1. - slope $\frac{1}{2}$, - SP_m , - SP_a , - $Rusanov$.

Errors in L^1 -norm against CPU time are displayed on figure 6 for u_1 and u_2 (ρ_1 and ρ_2 respectively present the same trends). Considering a given error, one observes that SP_a is the most efficient scheme. Even if SP_m is more efficient than $Rusanov$ on phase 2, it suffers from a lack of accuracy on the fastest phase (i.e. phase 1) and the use of material time steps is not appropriate for this test case. Indeed, one considers only fast waves so that the optimal regime is obtained with acoustic time steps.

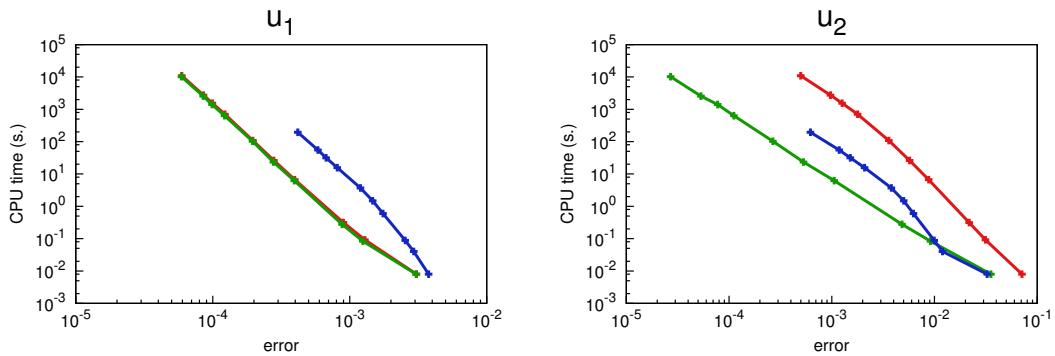
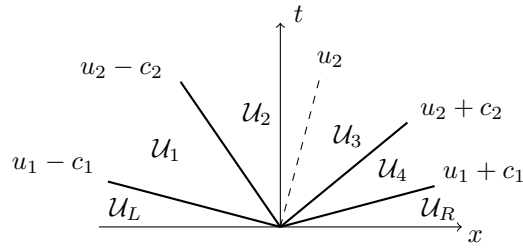


Figure 6: Error in L^1 -norm against CPU time for test case 1. - SP_m , - SP_a , - $Rusanov$.

4.2.2 Test case 2: a complete case with all the waves

In this case, all the waves are considered. The analytical solution contains two shocks for each phase traveling with the acoustic waves and one contact discontinuity in $\lambda_1 = u_2$ where h_1 jumps, see figure 7 and 8.



Variable	\mathcal{U}_L	\mathcal{U}_1	\mathcal{U}_2	\mathcal{U}_3	\mathcal{U}_4	\mathcal{U}_R
h_1	0.5	0.5	0.5	0.5023747	0.5023747	0.5023747
ρ_1	998.11150	998.16140	998.16140	998.16240	998.16240	998.06259
u_1	10.0	9.9254584	9.9254584	9.8225555	9.8225555	9.6734610
ρ_2	1.204	1.204	1.2642	1.2601362	1.2349335	1.2349335
u_2	5.0	5.0	-11.838960	-11.838960	-18.826134	-18.826134

Figure 7: Wave structure, initial conditions ($\mathcal{U}_L, \mathcal{U}_R$) and intermediate states $(\mathcal{U}_k)_{k=1,4}$ for test case 2.

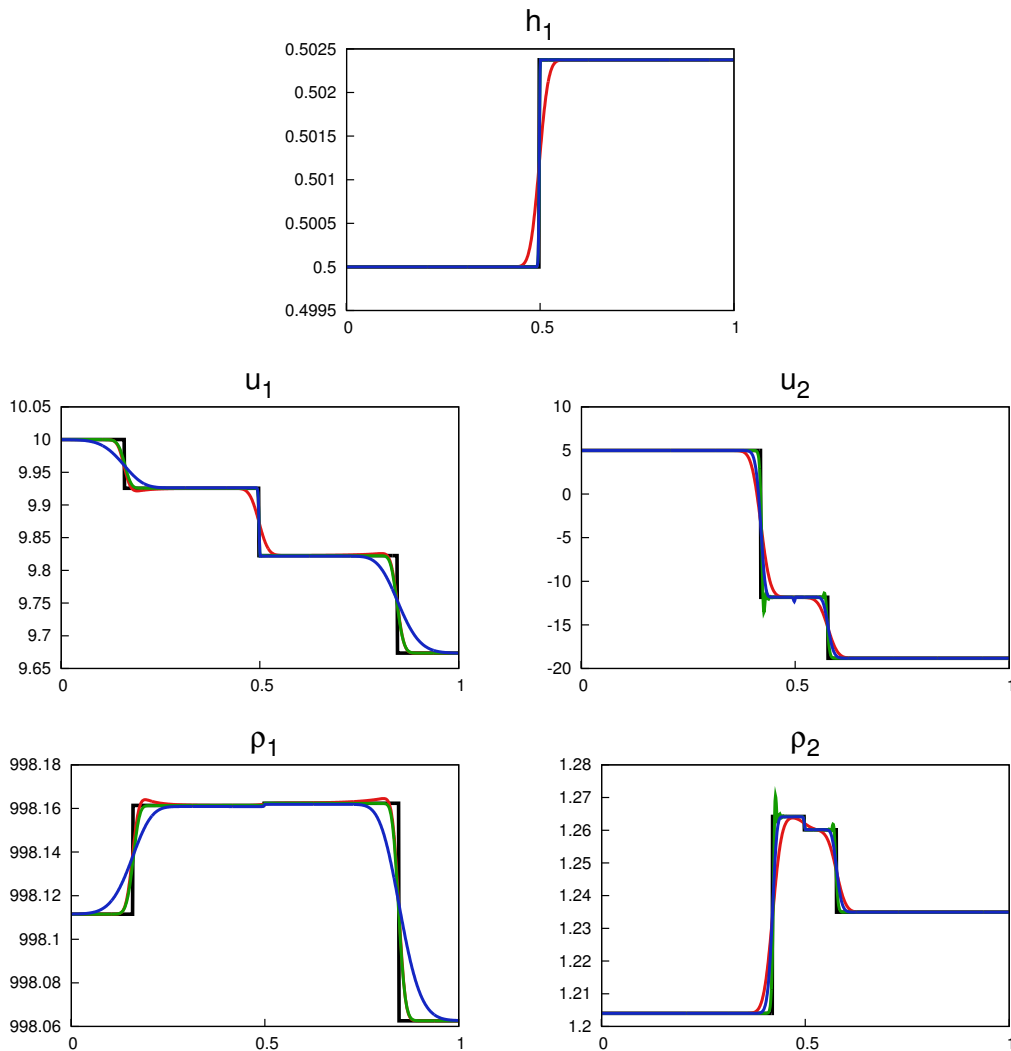


Figure 8: Approximate solution for test case 2 at $T = 23.10^{-5}$ s. with 1000 cells. - Exact solution, - SP_m , - SP_a , - Rusanov.

The fields at $T = 23.10^{-5}$ s. with 1000 cells and the errors are displayed respectively on figures 8 and 9. Despite the great complexity of this second test case, one observes that the intermediate states are correctly captured. The same trends as in the previous test case are observed. SP_a presents the best accuracy for both phases while SP_m is more diffusive for phase 1 and behaves slightly better than $Rusanov$ for phase 2. In particular, the contact discontinuity traveling at material speed is better captured using the implicit-explicit scheme. Overshoots are still observed with SP_a on the fields but they are bounded in L^∞ -norm and do not preclude the convergence. Regarding the order of convergence on figure 9, the expected convergence rate $\frac{1}{2}$ is obtained.

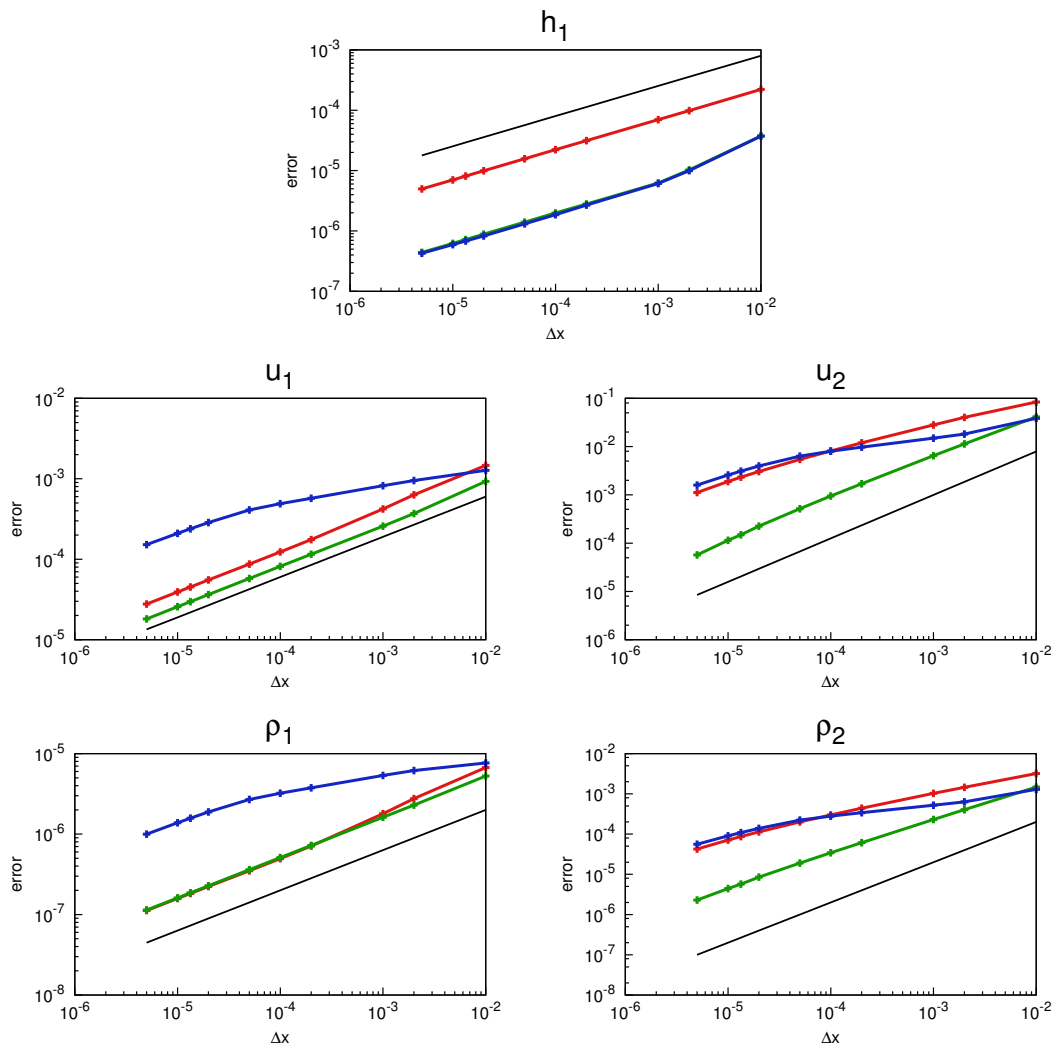


Figure 9: Errors in L^1 -norm for test case 2. - slope $\frac{1}{2}$, - SP_m , - SP_a , - $Rusanov$.

The test case is a mix between the (slow) material wave in $\lambda_1 = u_2$ and the fast acoustic waves in $\lambda_k = u_k \pm c_k$. On one hand, focusing on h_1 which is (in theory) directly affected by the slow wave, figure 10 shows that SP_m is the most efficient. As expected, the use of material time steps is the best choice to approximate material waves. On the other hand, regarding u_1 , the velocity of the fastest phase which is affected by all the waves, SP_m yields the worst efficiency while the use of acoustic time steps through SP_a is the best choice. Regarding u_2 , the best efficiency is still obtained with SP_a while SP_m is more efficient than $Rusanov$. Thus, the efficiency results strongly depend on the wave under consideration and consequently on the related variables.

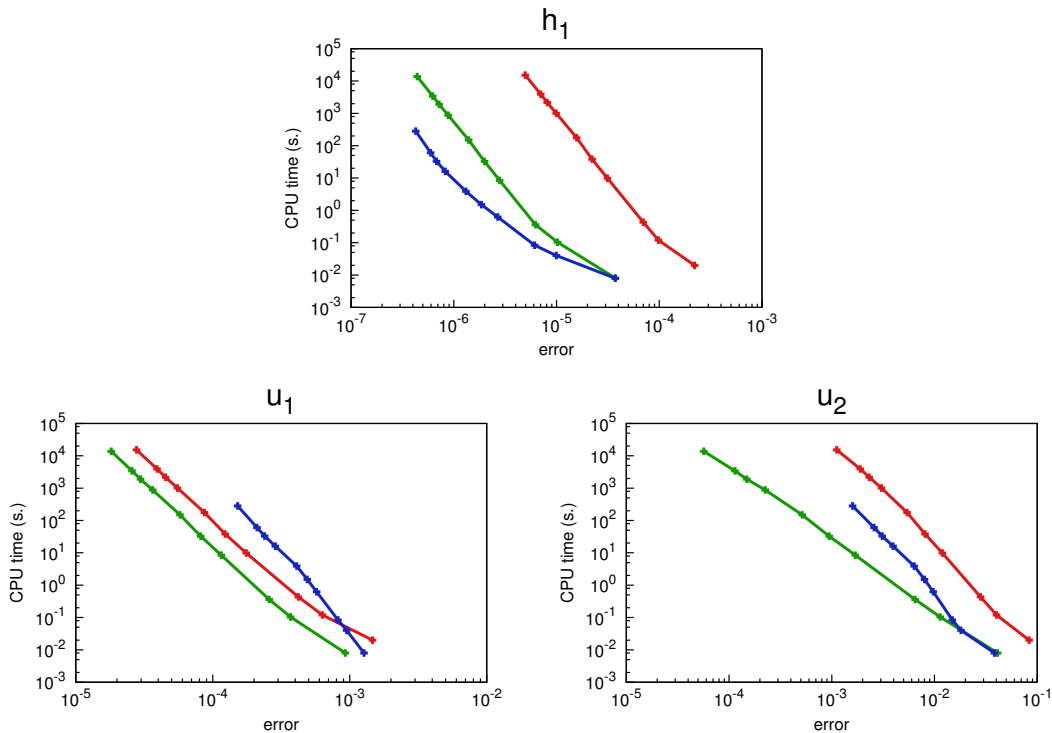


Figure 10: Error in L^1 -norm against CPU time for test case 2. - SP_m , - SP_a , - Rusanov.

4.3 Comments

The results presented in this section deal with an implicit-explicit splitting scheme, namely **SP**, regarding the convective part of the compressible two-layer model. **SP** is used with *acoustic* time steps as well as *material* time steps and compared with a classical explicit Rusanov scheme which requires *acoustic* time steps. The considered test cases highlight the following comments:

- Stability and convergence towards relevant shock solutions are obtained for **SP** and Rusanov.
- **SP** with acoustic time steps (SP_a) is the most efficient regarding the (fast) acoustic waves.
- **SP** with material time steps (SP_m) is the most efficient regarding the (slow) material wave.

At the end, the best accuracy is obtained with SP_a while a competition in terms of variables is observed regarding the efficiency: best efficiency on the variables $(\rho_1, u_1, \rho_2, u_2)$ given by SP_a or best efficiency on the variable h_1 given by SP_m . Thus, one has to determine the most profitable variant regarding all the fields and the considered test case.

Those comments focus on the convective part of the model. In order to pursue this analysis, the full compressible two-layer model is considered in the next section with the aim of including the source terms in the **SP** framework. Indeed, relaxation phenomena encountered in physical configurations may have great influence regarding the system behavior.

5 Extension to the full system with source terms

In this section, one deals with the source terms of the compressible two-layer model detailed in (2.1), namely the pressure relaxation and the velocity relaxation. Numerical experiments are performed considering a dam-break problem in addition to a mixed flow test case which involves a transition to the pressurized regime through a pipe filling.

5.1 Splitting approach

Regarding the pressure relaxation term, $\lambda_p(P_I - P_2)$, one may easily demonstrate that the associated relaxation process, i.e $P_I \xrightarrow[t \rightarrow \infty]{} P_2$, is very fast for air-water flows. The proposed approach is driven by this behavior and consists in plugging the source terms in (\mathcal{S}_1) which becomes (\mathcal{S}_1^s) . Thus, (\mathcal{S}_2) is unchanged and the proposed splitting reads:

$$\begin{aligned}
 (\mathcal{S}_1^s) \quad & \frac{\partial h_1}{\partial t} + u_2 \frac{\partial h_1}{\partial x} = \lambda_p(P_I - P_2), \\
 & \frac{\partial m_k}{\partial t} = 0, \\
 & \frac{\partial m_k u_k}{\partial t} = (-1)^k \lambda_u (u_1 - u_2). \\
 (\mathcal{S}_2) \quad & \frac{\partial h_1}{\partial t} = 0, \\
 & \frac{\partial m_k}{\partial t} + \frac{\partial m_k u_k}{\partial x} = 0, \\
 & \frac{\partial m_k u_k}{\partial t} + \frac{\partial m_k u_k^2}{\partial x} + \frac{\partial h_k P_k}{\partial x} - P_I \frac{\partial h_k}{\partial x} = 0.
 \end{aligned}$$

The overall scheme which includes the source terms is denoted \mathbf{SP}^s . The latter slightly differs from \mathbf{SP} regarding the first sub-system (\mathcal{S}_1^s) which as before, updates the state variable W_i from W_i^n to W_i^* . The associated numerical scheme is detailed below. Note that (\mathcal{S}_2) is treated as in subsection 3.4 such that no details are provided in the current section.

5.2 Numerical treatment of the source terms

5.2.1 Pressure relaxation

The transport equation on h_1 is discretized as in subsection 3.3, see (3.7), where the source term is added implicitly for stability reasons. It writes:

$$h_{1,i}^* - h_{1,i}^n + \Delta t \int_{x_{i-\frac{1}{2}}}^{x_{i+\frac{1}{2}}} u_2^n \frac{\partial h_1^n}{\partial x} dx = \Delta t \lambda_{p,i}^* (P_{I,i}^* - P_{2,i}^*), \quad (5.2)$$

where upwind fluxes are used for the convection term.

As m_k is constant w.r.t. time in (\mathcal{S}_1^s) , it yields $P_{2,i}^* = P_2(\rho_{2,i}^*) = P_2\left(\frac{m_{2,i}^n}{H-h_{1,i}^*}\right)$, $P_{I,i}^* = P_1\left(\frac{m_{1,i}^n}{h_{1,i}^*}\right) - m_{1,i}^n \frac{g}{2}$ and (5.2) is equivalent to

$$f(h_{1,i}^*) = 0 \quad (5.3)$$

where

$$f(y) = y - h_{1,i}^n + \Delta t \int_{x_{i-\frac{1}{2}}}^{x_{i+\frac{1}{2}}} u_2^n \frac{\partial h_1^n}{\partial x} dx - \Delta t \lambda_{p,i}^* \left(P_1\left(\frac{m_{1,i}^n}{y}\right) - m_{1,i}^n \frac{g}{2} - P_2\left(\frac{m_{2,i}^n}{H-y}\right) \right). \quad (5.4)$$

One may easily demonstrate that f is strictly increasing on $[0; H]$ with the limits $f \xrightarrow[0^+]{} -\infty$ and $f \xrightarrow[H^-]{} +\infty$, such that (5.3) admits a unique solution $h_{1,i}^*$ on $[0; H]$. In practice, $\lambda_{p,i}^* = \lambda_{p,i}^n$ as $m_{k,i}^* = m_{k,i}^n$, see appendix A.1. Thus, $h_{1,i}^*$ can be obtained using classical numerical methods devoted to nonlinear equations such as the bisection or Newton's method. In addition, note that in this framework, there is no need for CFL conditions to ensure the positivity of $h_{k,i}^*$.

5.2.2 Velocity relaxation

Once $h_{k,i}^*$ is obtained, the remaining unknown is $u_{k,i}^*$, given by the last equation of (\mathcal{S}_1^s) . As for the pressure relaxation, the source term is treated implicitly except for the λ_u parameter. Indeed, the latter may include

complex functions depending on the state variable and accounting for friction effects, see appendix A.2. Using the fact that m_k is constant w.r.t. time, the proposed implicit scheme writes:

$$m_{k,i}^n (u_{k,i}^* - u_{k,i}^n) = (-1)^k \Delta t \lambda_{u,i}^n (u_{1,i}^* - u_{2,i}^*). \quad (5.5)$$

Combining (5.5) for $k = 1, 2$, one obtains the following *nonsingular* 2×2 system

$$\begin{pmatrix} m_{1,i}^n + \Delta t \lambda_{u,i}^n & -\Delta t \lambda_{u,i}^n \\ -\Delta t \lambda_{u,i}^n & m_{2,i}^n + \Delta t \lambda_{u,i}^n \end{pmatrix} \begin{pmatrix} u_{1,i}^* \\ u_{2,i}^* \end{pmatrix} = \begin{pmatrix} (m_1 u_1)_i^n \\ (m_2 u_2)_i^n \end{pmatrix}. \quad (5.6)$$

This system can be solved directly and one obtains an explicit relation for $u_{k,i}^*$.

At this point, (S_1^s) is solved accounting for the relaxation processes. (S_2) is then solved as in section 3.4 to obtain the updated state variable W_i^{n+1} . In order to assess this method, two test cases are considered in the next subsection.

5.3 Numerical results

In the sequel, numerical tests are performed with SP_a^s and SP_m^s which denote respectively the SP^s scheme with *acoustic* and *material* time steps. As in section 4, the acoustic time step is denoted Δt_a and defined in (4.1). The material time step is denoted Δt_m and defined in (4.2) except that the CFL condition regarding the positivity of h_k , see (3.8), can be ignored when including the pressure relaxation term. In addition, one considers the **Rusanov** scheme applied to (S_0) where the source terms are classically treated in a second step involving only ODEs, see [21]. The latter scheme is denoted **Rusanov**^s hereafter to be consistent in the notations.

5.3.1 Dam-break test case

A common way to deal with free-surface flows is to use the well-known Saint-Venant or shallow-water equations, see [19]. In a few words, this model is a *one-layer* model resulting from a depth averaging process on the Euler set of equations and assuming a thin layer of incompressible fluid (water for instance) with hydrostatic pressure law. Particularly, it admits an analytical solution for the so-called dam-break problem detailed below. Note that this classical approach is used in [5] to model the free-surface regime in pipe flows without computing the air phase.

In the following, it is proposed to consider the dam-break test case for the compressible two-layer model and to compare the results with the reference solution provided by the Saint-Venant system for the single water layer. Indeed, one can expect to obtain the same kind of solution as the derivation processes are very close and the compressibility of water as well as the additional air layer should have a minor influence here.

The (low-Mach) dam-break problem

The dam-break problem is a Riemann problem where the initial condition is a discontinuity on h_1 with constant density and zero speed, see figure 11. Regarding the water layer, the analytical solution of the incompressible shallow-water system, denoted SW_{ref} hereafter, provides the evolution in time and space for h_1 and u_1 which contains a rarefaction wave propagating to the left and a shock wave propagating to the right.

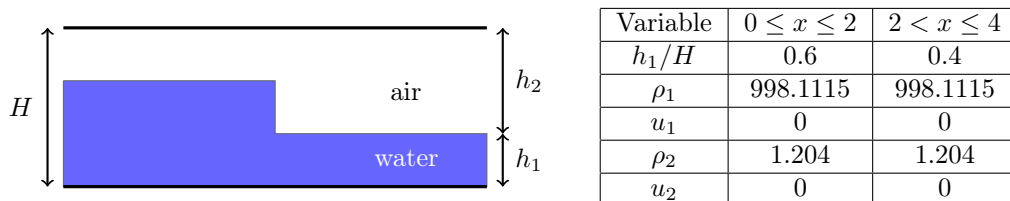


Figure 11: Initial conditions for the dam-break problem

In the context of the compressible two-layer model, this test case can be interpreted as a low Mach number flow. Indeed, introducing the Mach number M defined as:

$$M = \max_{k=1,2} \left| \frac{u_k}{c_k} \right|, \quad (5.7)$$

one has $M \ll 1$ which typically makes the solutions difficult to approximate accurately.

Implementation

The solutions are computed on the domain $[0,4]$ of the x -space where the initial conditions are given on figure 11. Regarding the boundary conditions, one imposes homogeneous Neumann conditions at the inlet and outlet. The fields are presented on a 4000 cells mesh at time $T = 0.11$ s. Two configurations are considered regarding the Mach number value: $M \sim 10^{-2}$ and $M \sim 10^{-3}$. Note that this range of Mach number fits with realistic pipe flows.

Results

On figure 12, SP_a^s is compared with $Rusanov^s$ at $M \sim 10^{-3}$. As a first comment, note that both schemes seem to follow the SW_{ref} solution regarding h_1 and u_1 , which is the expected trend for the compressible two-layer model since the air layer has minor influence here. In addition, admitting SW_{ref} as a reference solution, one observes that SP_a^s is more accurate than $Rusanov^s$ as for the homogeneous test cases presented in section 4.

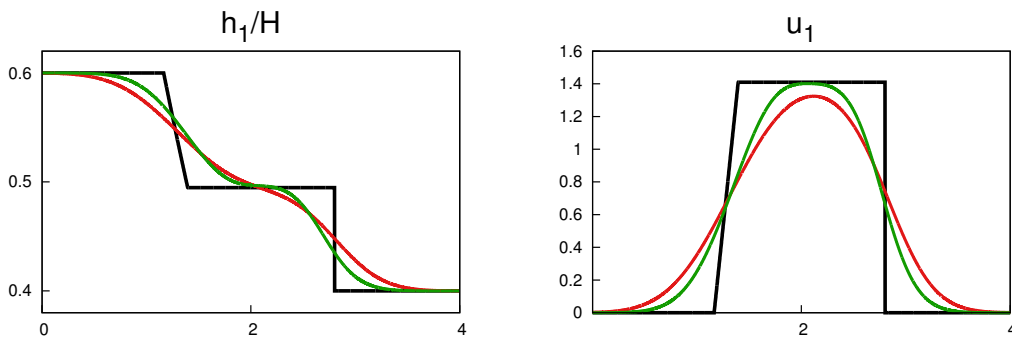


Figure 12: Approximate solution at $T = 0.11$ s. with $M \sim 10^{-3}$ and 4000 cells. - SW_{ref} , - SP_a^s , - $Rusanov^s$.

On figure 13, SP_m^s is compared with $Rusanov^s$ at $M \sim 10^{-3}$. In practice $\Delta t_m \sim 100\Delta t_a$ and one observes that SP_m^s is unable to restore the SW_{ref} solution. The solution obtained for h_1 is totally inaccurate so that the comments given in subsection 4.3 cannot be extended to SP_m^s . Refining the mesh, one obtains the expected structure but SP_m^s is inefficient for all the variables compared to SP_a^s and $Rusanov^s$. Consequently, the use of material time steps with the proposed implicit-explicit splitting scheme seems to be too sharp regarding such a low Mach test case.

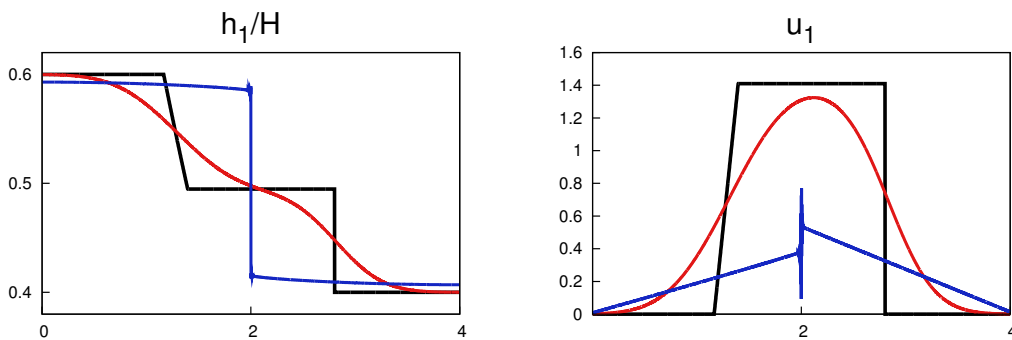


Figure 13: Approximate solution at $T = 0.11$ s. with $M \sim 10^{-3}$ and 4000 cells. - SW_{ref} , - SP_m^s , - $Rusanov^s$.

When the Mach number is multiplied by a factor 10, $M \sim 10^{-2}$ and \mathbf{SP}_m^s is able to restore the structure of the SW_{ref} solution although the profiles are very diffusive, see figure 14. \mathbf{SP}_a^s is still more accurate than $\mathbf{Rusanov}^s$ but diffusivity is also observed. At last, those results illustrate the difficulties to handle two-phase low Mach solutions with even more challenges at large time steps.

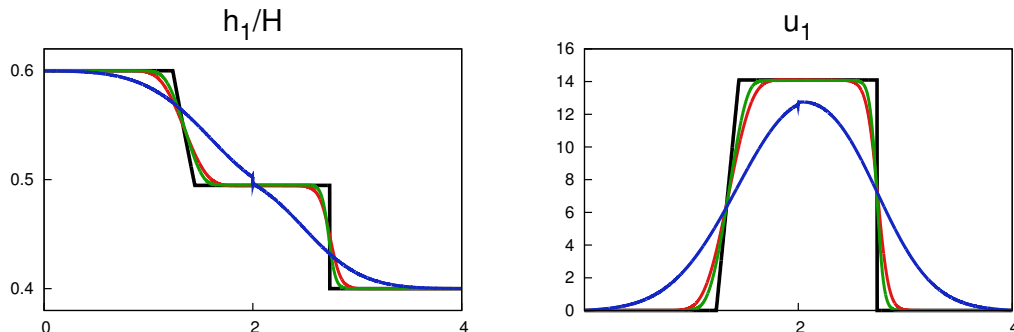


Figure 14: Approximate solution at $T = 0.11$ s. with $M \sim 10^{-2}$ and 4000 cells. - SW_{ref} , - \mathbf{SP}_a^s , - \mathbf{SP}_m^s , - $\mathbf{Rusanov}^s$.

5.3.2 A first attempt to deal with mixed flows: pipe filling test case

In this test case, one considers a more complex configuration which involves a transition from the free-surface regime to the pressurized regime, namely a mixed flow. As exposed in [16], the compressible two-layer model degenerates correctly towards an isentropic Euler set of equations for the water phase when the height of the air phase goes to zero. The latter equations are commonly used to describe pressurized flows but in our framework, one has to handle numerically the vanishing air phase which may be a tough challenge.

In order to enable a transition to the pressurized regime, one considers a sloping pipe with a wall boundary condition at the outlet and a classical homogeneous Neumann boundary condition at the inlet. The initial conditions are the same as the ones used for the dam-break test case, see figure 11, except that the pipe is inclined by 20 degrees to the horizontal. The computations are still done on the domain $[0,4]$ of the x -space with a 4000 cells mesh. There is no analytical solution but the idea is to obtain *qualitative* results. Note that the exposed results mainly involve ongoing work.

On figure 15, one displays a snapshot w.r.t. time regarding the height of the water phase. The $\mathbf{Rusanov}^s$ scheme is used and one obtains encouraging results. Indeed, the vanishing air phase configuration seems to be handled providing a realistic qualitative behavior. However, the \mathbf{SP}^s scheme is not able to reproduce this behavior. As a first explanation, one notices that when the height of the air phase goes to zero, the matrix A_2^* involved in (3.16) to compute the air pressure goes as well to zero and the system becomes hard to solve numerically. In order to cope with that issue, the use of preconditionning techniques could be an area of investigation.

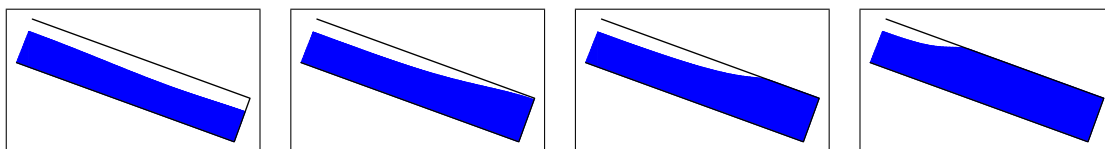


Figure 15: Snapshots w.r.t. time for the pipe filling case using the $\mathbf{Rusanov}^s$ scheme. Height of the water phase in blue.

This test may illustrate the ability of the compressible two-layer model to handle mixed flows at least using a diffusive scheme as the $\mathbf{Rusanov}^s$ scheme. Further investigations have to be led in order to adapt the \mathbf{SP}^s scheme to the vanishing phases configuration.

6 Conclusion and further works

An implicit-explicit splitting scheme, namely **SP**, is presented to approximate the solutions of the compressible two-layer model developed in [16]. The CFL condition associated to this scheme relies on material velocities but numerical experiments are performed using *acoustic* as well as *material* time steps. In short, adding the Rusanov scheme for comparison, the best accuracy is obtained with the proposed scheme used with *acoustic* time steps. When used with *material* time steps, efficiency on the slow waves and stability are obtained regarding analytical solutions of the convective part.

More precisely, one obtains convergent approximations of analytical discontinuous solutions regarding the convective part. As expected, the use of *acoustic* time steps leads better efficiency on fast waves while the *material* time steps yields better efficiency on slow waves. When considering the source terms and the (low-Mach) dam-break problem, the latter comments cannot be extended. The use of *acoustic* time steps leads to encouraging results which meet the expected behavior of the compressible two-layer model. However, the use of *material* time steps in this context yields unsatisfactory results. Thus, the proposed scheme may not be fitted to deal correctly with the full system at large time steps and low Mach number.

With the aim of improving the performances of the implicit-explicit splitting approach at large time steps, ongoing work includes the study of the model at the continuous level and particularly its asymptotic limit regarding relaxation phenomena and low Mach number flow. The goal is to obtain a limit model which could guide the derivation of an efficient scheme at large time steps. Note that this kind of approach provides interesting results regarding, for instance, the Euler model and the so-called *asymptotic preserving* schemes, see [9] among others.

Dealing with industrial applications, one may also consider vanishing phases occurring in pressurized flows and entrapped air pockets. A first attempt to address this challenge is done herein with the pipe filling test case. The explicit Rusanov scheme displays interesting qualitative results. Regarding implicit schemes and the results provided by **SP**, the work under progress focuses on preconditioning as well as threshold techniques to ensure the transition. At last, experimental results which involve such configurations, see for instance [7, 23, 10], will be used to validate the numerical scheme and the model.

Acknowledgments. This work has been partially funded by ANRT and EDF through an EDF-CIFRE contract 749/2014. Computational facilities were provided by EDF.

Appendix A Closure laws for the source terms

A.1 Pressure relaxation

In order to determine the time scale associated to pressure relaxation, one considers in [18] the evolution of a bubble in an infinite medium using the Rayleigh-Plesset equation. Regarding the source term $\lambda_p(P_I - P_2)$ in (2.1), the latter approach is extended to our framework so that the λ_p function reads:

$$\lambda_p = \frac{3}{4\pi\mu_1} \frac{m_1 m_2}{H\rho_{1,\text{ref}}\rho_{2,\text{ref}}}, \quad (\text{A.1})$$

where μ_1 is the dynamic viscosity of phase 1 and $\rho_{k,\text{ref}}$ is the reference density used to calibrate the pressure law of phase k .

A.2 Velocity relaxation

Regarding the averaged momentum conservation equation (2.1c), the source term $\lambda_u(u_2 - u_1)$ accounts for friction effects between phases. Thus, following the work developed in [26], the latter is modeled as a classical interfacial drag force and λ_u writes:

$$\lambda_u = \frac{h_1 h_2}{2H^2} f_i \rho_2 |u_2 - u_1|, \quad (\text{A.2})$$

where $f_i = C_i Re_i^{-n}$ is the so-called friction factor. Re_i is defined as $Re_i = \frac{(u_2 - u_1)h_2}{\nu_2}$ with ν_2 the kinematic viscosity of phase 2. According to the correlations proposed in [26], $C_i = 0.046$ and $n = 0.25$ for $Re_i > 2100$ while $C_i = 16$ and $n = 1$ for $Re_i \leq 2100$.

References

- [1] A. Ambroso, C. Chalons, and P.-A. Raviart. A Godunov-type method for the seven-equation model of compressible two-phase flow. *Computers & Fluids*, 54:67–91, 2012.
- [2] A. Andiranov and G. Warnecke. The Riemann problem for the Baer-Nunziato two-phase flow model. *J. Comput. Phys.*, 195(2):434–464, 2004.
- [3] M. R. Baer and J. W. Nunziato. A two phase mixture theory for the deflagration to detonation (DDT) transition in reactive granular materials. *Int. J. Multiphase Flow*, 12(6):861–889, 1986.
- [4] R. Baraille, G. Bourdin, F. Dubois, and A.-Y. Le Roux. A splitted version of the Godunov scheme for hydrodynamic models. *C. R. Acad. Sci. Paris*, 314(1):147–152, 1992.
- [5] C. Bourdarias and S. Gerbi. A finite volume scheme for a model coupling free surface and pressurised flows in pipes. *J. Comput. Appl. Math.*, 209:1–47, 2007.
- [6] T. Buffard and J.-M. Hérard. A conservative fractional step method to solve non-isentropic Euler equations. *Comput. Methods Appl. Mech. Engrg.*, 144:199–225, 1997.
- [7] H. Capart, X. Sillen, and Y. Zech. Numerical and experimental water transients in sewer pipes. *J. Hydraul. Res.*, 35(5):659–672, 1997.
- [8] C. Chalons, F. Coquel, S. Kokh, and N. Spillane. Large time-step numerical scheme for the seven-equation model of compressible two-phase flows. *Springer Proceedings in Mathematics and Statistics*, 4:225–233, 2011.
- [9] C. Chalons, M. Girardin, and S. Kokh. Large time-step and asymptotic preserving numerical schemes for the gas dynamics equations with source terms. *SIAM J. Sci. Comput.*, 35(6):a2874–a2902, 2013.
- [10] C. D. Chosie, T. M. Hatcher, and J. G. Vasconcelos. Experimental and numerical investigation on the motion of discrete air pockets in pressurized water flows. *J. Hydraul. Eng.*, 140(8):25–34, 2014.
- [11] F. Coquel, J.-M. Hérard, and K. Saleh. A splitting method for the isentropic Baer-Nunziato two-phase flow model. *ESAIM: Proceedings*, 38(3):241–256, 2012.
- [12] F. Coquel, J.-M. Hérard, K. Saleh, and N. Seguin. A robust entropy-satisfying finite volume scheme for the isentropic Baer-Nunziato model. *ESAIM: Math. Model. and Numer. Analysis*, 48:165–206, 2013.
- [13] F. Coquel, Q.-L. Nguyen, M. Postel, and Q.-H. Tran. Entropy-satisfying relaxation method with large time-steps for Euler ibvps. *Math. Comp.*, 79:1493–1533, 2010.
- [14] P. Degond and M. Tang. All speed scheme for the low mach number limit of the isentropic Euler equation. *Communications in Computational Physics*, 10:1–31, 2011.
- [15] V. Deledicque and M.V. Papalexandris. An exact Riemann solver for compressible two-phase flow models containing non-conservative products. *J. Comput. Phys.*, 222(1):217–245, 2007.
- [16] C. Demay and J.-M. Hérard. A compressible two-layer model for transient gas-liquid flows in pipes. *Continuum Mech. Thermodyn.*, 2016.
- [17] T. Gallouët, J.-M. Hérard, and N. Seguin. Numerical modeling of two-phase flows using the two-fluid two-pressure approach. *Math. Models Methods Appl. Sci.*, 14(15):663–700, 2004.
- [18] S.L. Gavriluk. The structure of pressure relaxation terms : one-velocity case. *EDF report H-I83-2014-00276-EN*, 2014.
- [19] J.-F. Gerbeau and B. Perthame. Derivation of viscous Saint-Venant system for laminar shallow water; numerical validation. *Discrete Contin. Dyn. Syst. Ser. B*, 1:89–102, 2001.
- [20] J. Haack, S. Jin, and J.G. Liu. An all-speed asymptotic preserving method for the isentropic Euler and navier-stokes equations. *Communications in Computational Physics*, 12:955–980, 2012.

-
- [21] J.-M. Hérard and O. Hurisse. A fractional step method to compute a class of compressible flows with micro-inertia. *Computers & Fluids*, 55:57–69, 2012.
- [22] S. Noelle, G. Bispen, K. Arun, M. Lukacova-Medvidova, and C.D. Munz. An asymptotic preserving all mach number scheme for the Euler equations of gas dynamics. *IGPM Preprint*, 348, 2012.
- [23] I.W.M. Pothof and F.H.L.R. Clemens. Experimental study of air-water flow in downward sloping pipes. *Int. J. Multiphase Flow*, 37(3):278–292, 2011.
- [24] V. H. Ransom and D. L. Hicks. Hyperbolic two-pressure models for two-phase flow. *Journal of Computational Physics*, 53:124–151, 1984.
- [25] D. W. Schwendeman, C. W. Wahle, and A. K. Kapila. The Riemann problem and a high-resolution Godunov method for a model of compressible two-phase flow. *J. Comput. Phys.*, 212(2):490–526, 2006.
- [26] Y. Taitel and A.E. Dukler. A model for predicting flow regime transitions in horizontal and near horizontal gas-liquid flow. *AIChE J.*, 22:47–55, 1976.
- [27] S.-A. Tokareva and E.-F. Toro. HLLC-type Riemann solver for the Baer-Nunziato equations of compressible two-phase flow. *J. Comput. Phys.*, 229(10):3573–3604, 2010.
- [28] S.-A. Tokareva and E.-F. Toro. A flux splitting method for the Baer–Nunziato equations of compressible two-phase flow. *J. Comput. Phys.*, 323:45–74, 2016.
- [29] E.F. Toro and M.E. Vázquez-Cendón. Flux splitting schemes for the Euler equations. *Computers & Fluids*, 70:1–12, 2012.
- [30] V. V Rusanov. Calculation of interaction of non-steady shock waves with obstacles. *J. Comp. Math. Phys.*, 1:267–279, 1961.